Soroush Shahnia, Junaiz Rehmen, David G. Lancaster, Tanya M. Monro, Heike Ebendorff-Heidepriem, Drew Evans and Shahraam Afshar V.

Towards new fiber optic sensors based on the vapor deposited conducting polymer PEDOT:Tos

Optical Materials Express, 2019; 9(12):4517-4531

DOI: http://dx.doi.org/10.1364/OME.9.004517

Research Article | Vol. 9, No. 12 / 1 December 2019 / Optical Materials Express 4517
Optical Materials EXPRESS

Towards new fiber optic sensors based on the vapor deposited conducting polymer PEDOT:Tos

SOROUSH SHAHNIA,[1] JUNAIZ REHMEN,[2] DAVID G. LANCASTER,[1] TANYA M. MONRO,[1] HEIKE EBENDORFF-HEIDEPRIEM,[3] DREW EVANS,[2,4] AND SHAHRAAM AFSHAR V.[1,3,5]

[1]*Laser Physics and Photonic Devices Laboratories, School of Engineering, University of South Australia, SA 5095, Australia*
[2]*Future Industries Institute, University of South Australia, SA 5095, Australia*
[3]*ARC Center of Excellence for NanoScale BioPhotonics, Institute for Photonics and Advanced Sensing, The University of Adelaide, Adelaide 5005, Australia*
[4]*Drew.Evans@unisa.edu.au*
[5]*Shahraam.AfsharVahid@unisa.edu.au*

Abstract: Conducting polymers are widely researched in terms of both their electrical and optical properties. These optical properties are typically observed on the macroscopic (mm^2-cm^2) scale using techniques such as UV-Vis-NIR spectroscopy. To broaden their application, fabrication and characterization of conducting polymers on the microscale (μm^2) are required. In this paper, microscale poly(3,4-ethylenedioxytiophene)-tosylate (PEDOT:Tos) layers were vapor deposited at the tip of a single mode optical fiber. This was done without the need for intermediate layers such as Indium Tin Oxide commonly used in electropolymerization. The optical properties and behavior of PEDOT:Tos below thicknesses of 500 nm were investigated. Laser-induced damage (LID) behavior of the PEDOT:Tos layer was observed for different intensities of CW or pulsed near infrared light (primarily at 1550 nm). A mathematical model based on energy deposition and the laser-induced damage threshold (LIDT) for low intensity light radiation was developed. It was shown that LID can be avoided by applying irradiance below 31.8 W/mm^2 for both CW and pulsed laser. Understanding of LIDT has implications for the use of conducting polymers in new optical fiber sensing applications.

1. Introduction

Thin film conducting polymers (CPs) are a relatively new generation of material with attractive properties and behavior that can include high electrical conductivity and optical transparency, electro-catalytic behavior, mechanical flexibility, and lightweight. They offer unique combinations of properties not possible with other materials (such as metals, and ceramics) [1–8]. Since their discovery in the 1970s, studies have been mainly focused on developing facile synthesis processes for producing CPs with enhanced electrical [9,10], electrochromic [8,11,12], and electrocatalytic [3,4,13] properties primarily on macroscopic rigid substrates such as glass sheet. Owing to its properties, poly(3,4-ethylenedioxythiophene) (PEDOT) is one of the most studied CP's. It has been utilised for demonstrating applications including light emitting diodes (OLED) [14], optical displays [6], photovoltaic devices [15] and sensors [16].

PEDOT and more specifically PEDOT doped with the tosylate anion (PEDOT:Tos) synthesized via the vapor phase polymerization (VPP) technique [17], has gathered the recent interest of researchers [18–20]. To a large extent, this has been due to the polymer's chemical and environmental stability in its doped states, as well as high electrical conductivity [20] and large

#374675 https://doi.org/10.1364/OME.9.004517
Journal © 2019 Received 27 Aug 2019; revised 12 Oct 2019; accepted 27 Oct 2019; published 4 Nov 2019

Optical Materials EXPRESS

optical transmission changes that can be achieved with redox switching [21]. In its oxidized state (doped), PEDOT is almost visibly transparent (light blue in color). In the reduced state (dedoped), PEDOT changes to an opaque material that is dark blue in color. This characteristic of PEDOT makes it suitable for optical applications such as in electrochromic devices [22] and possibly in optical sensors. In general terms, optical sensing requires interaction between light and the sensing material. When the sensing material responds to an external stimulus, light can be used to interrogate and measure this change - therefore linking the optical measurement to the external stimuli. An essential aspect of optical sensing is the means by which light is guided to and from the sensing material. Optical fibers are an excellent example of a way to guide light to a volume or point of interest for sensing [23]. In one configuration optical material is coated on the side or at the tip of the fiber, which are typically inorganic material. Fiber tip fabrication and side coating are used in many recent sensing applications such as Er^{3+}/Yb^{3+} doped tellurite temperature sensor for in vivo measurements [24], hydrogen sensors using palladium coated fiber optics [25] and polymer functionalization of exposed-core microstructured optical fibers for sensing Al [26].

Microscale patterning of PEDOT has been achieved using various techniques such as inkjet printing [27], dip-pen nanolithography [28], and UV-lithography [29]. However, these studies focus on creating microscale patterns on largely macroscopic and often planar substrates. When scaling fabrication down to smaller length scales the method of synthesis may need modification. Owing to structure-property relationships, the change in synthesis likely induces subtle changes in structure that lead to different properties. Beyond this, when applications are considered the microscale film can show behavior indicative of insufficient charge carriers. Put simply, certain underlying mechanisms may be inhibited or impaired because of a finite reservoir of charge carriers. As opposed to macroscopic films that appear as an infinite reservoir of charge carriers. Herein, we propose a novel fiber optic sensing architecture based on coating the tip of an optical fiber with VPP PEDOT:Tos. This is a novel architecture which allows exploring the unique electrochemical properties of PEDOT:Tos at the sub-micron length scale. This opens the possibility of integrating PEDOT with optical waveguides, including optical fibers and hence developing a variety of electro-optical devices. Integrating optical fibers with PEDOT:Tos as a sensing architecture allows combining the advantages of optical fibers such as immunity to electromagnetic fields, the possibility for in-vivo and distributed measurements with the electrochemical properties of PEDOT:Tos.

As a first step towards such a fiber optic sensor, we have developed a method to consistently deposit PEDOT:Tos layers with desired thicknesses on the tip of optical fibers. We have deposited sub-microscale thickness PEDOT:Tos coatings on optical fibers tip via vapor deposition. The vapor process removes the need for intermediate layers or materials - such as a transparent conductive layer commonly used for electropolymerization of PEDOT (doped with variety of anion [7,11]). In addition, by investigating the optical transmission and back-reflection of fibers with PEDOT:Tos tips, we have observed optical degradation of VPP PEDOT:Tos as irradiated by a CW laser during several hours. There is a threshold behavior in optical degradation of the VPP PEDOT:Tos and we specify the laser parameters to avoid laser-induced damage threshold (LIDT) and hence prolong the operation of the PEDOT:Tos tip fiber. Furthermore, based on the laser-induced energy changed in the VPP PEDOT:Tos layer, we have developed a model to explain its optical degradation and have verified the model with the experimental results. The model allows us to evaluate the time constant of the energy decay in the layer. This is an important parameter to identify the saturation regime of the layer, within which the optical response of the VPP PEDOT:Tos is constant. This information is invaluable for the development of fiber PEDOT:Tos based electro-optic devices and in particular PEDOT:Tos tip fiber optic sensors.

Optical Materials EXPRESS

2. Experiment

All the experiments conducted in the lab environment at 21 °C. PEDOT:Tos was deposited via VPP process at the tip of cleaned, and cleaved (≤1°) SMF-28 optical fiber. The deposition method includes a 4 step process: 1. Oxidant solution preparation, 2. Oxidant coating and splitting at the tip of the fiber, 3. VPP process and 4. Washing of unbound and unreacted monomers.

2.1. Materials

Iron tosylate ($Fe(Tos)_3$), in the form of Clevios CB54 (54 wt% in butanol), and 3,4-ethylenediox ythiophene (EDOT, Clevios V2) were obtained from Heraeus. Undenatured Ethanol (EtOH), Butanol (BuOH) and PEG-PPG-PEG (Pluronic P-123, Mw = 5800 g mol^{-1}) were obtained from Sigma Aldrich. All chemicals were used as is without further purification. SMF-28-100 optical fibers of core diameter 8.2 μm and cladding diameter of 125±0.7 μm, were obtained from thorlabs. SMF-28 optical fiber has consistent geometric properties, low attenuation and delivers high performance across a broad spectral range in the Telecom region.

2.2. Oxidant solution

An oxidant solution was prepared by mixing CB54 (3 parts by weight), PEG:PPG:PEG (3 parts by weight), EtOH (6 parts by weight) and BuOH (1 part by weight). These masses result in a solution of 270 mM $Fe(Tos)_3$ and 49 mM PEG:PPG:PEG in a 72% / 28% mixture by volume of EtOH / BuOH. The solution was heated at 70 °C for 30 minutes in a sealed container to aid dispersion of the PEG:PPG:PEG without loss of the alcohol solvent, and then left to cool to room temperature. This solution is the precursor layer required to directly synthesize the conducting polymer at the tip of the optical fiber.

2.3. Oxidant coating process

The volume of deposited oxidant solution was determined from analysis of microscope images from the side of the fiber after coating with the solution. The perimeter of the volume is used to calculate the deposited volume. The development of the dipping / splitting process to deposit small volumes of oxidant at the end of an optical fiber will be discussed in the results section 3.1.

2.4. Vapour phase polymerization

After the oxidant splitting process, the optical fiber was then placed inside a 115 L vacuum chamber oven (VD115 Binder, Germany) set to 35 °C. The chamber was evacuated to a pressure of 45 mbar, while a reservoir of EDOT monomer inside the chamber was heated at 45 °C. The condensation of monomer vapor over the oxidant coated substrate initiates the polymerization. Samples were removed from the chamber after 30 minutes and subsequently washed with EtOH to remove spent oxidant, unbound surfactant and unreacted monomers.

2.5. Thickness measurement

The thickness of each PEDOT layer was determined using a Focus Ion Beam/Scanning Electron Microscopy (FEI Helios Nanolab DualBeam FIB/SEM) by exposing a section of the PEDOT and optical fiber in its cross section and then imaging it (Fig. 1). To assist in this process, a platinum layer was deposited onto the PEDOT to produce a well-defined upper edge to the PEDOT for unambiguous measurement of thickness.

2.6. Elemental analysis

Elemental analysis of the coated film was carried out with the aid of Time-of-Flight Secondary Ion Mass Spectrometry (Physical Electronics Inc. Model 2100 PHI TRIFT IITM ToF-SIMS). Time of Flight Secondary Ion Mass Spectrometry (TOF-SIMS) is a surface sensitive analytical

Optical Materials EXPRESS

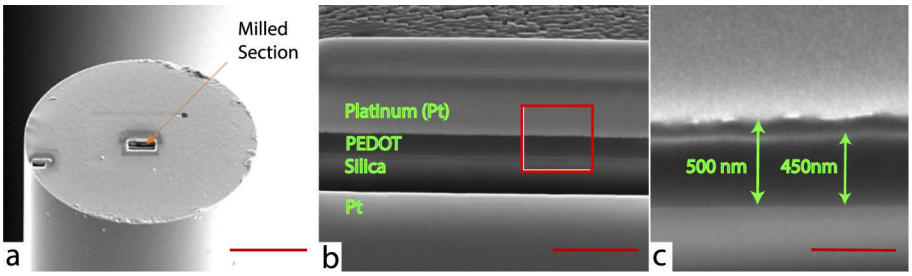

Fig. 1. SEM images of (a) PEDOT coated optical fiber milled using Focused Ion Beam with both milling and camera angle are 52°, (b) Cross-sectional image of the milled section of fiber, (c) thickness measured along the magnified cross-section with 50 nm uncertainty. Scale bars represent 50 μm, 2 μm and 500 nm for a, b and c respectively.

technique that provides detailed elemental and molecular information from the surface of a sample. Elemental and chemical mapping of the sample surface can be produced using this technique.

2.7. Experimental method and setup for optical characterization

Two main configuration were used to characterize the optical properties (reflectivity, transmission, absorption, and LIDT) of PEDOT layers deposited on the tip of an optical fiber (Fig. 2). In both cases, a circulator is used to measure the back-reflection. In Fig. 2(a), a fiber coupled distributed feedback CW laser diode (wavelength 1550 nm, model number GB5A016) connected to terminal 1 of the circulator is used. The PEDOT is deposited on one side of a bare single mode fiber (SMF-28). The other side on the bare fiber is spliced to a SMF-28 patch cord and connected to terminal 2 of the circulator. A position stage is used to bring the tip of the fiber close to the photodiode (Thorlabs S122C). To ensure that there is no contact between the PEDOT and the photodiode a USB plug and play microscope was used to monitor the location of the tip of the fiber. Transmission and back-reflection spectra are measured simultaneously through two photodiodes.

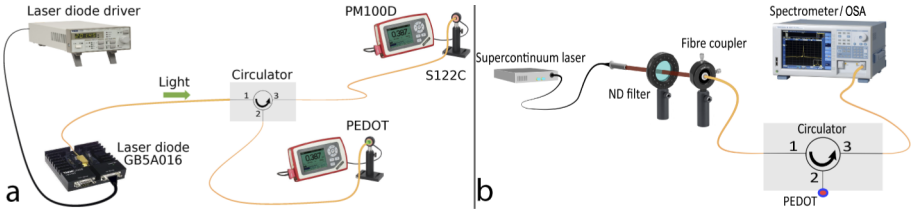

Fig. 2. (a) Experimental setup for measuring PEDOT:Tos degradation time based on optical transmission and back-reflection, (b) Experimental setup for PEDOT:Tos reflection broadband spectrum measurement.

A different setup (Fig. 2b) is required to measure the broadband reflection, in our case, between 1200 and 1700 nm of wavelength. In this setup, a fiber coupled super-continuum (SC) laser source is used as a broadband light source. The collimated beam out of the SC laser passes through the neutral-density filter to reduce the light intensity and is then coupled into the terminal 1 of the circulator. PEDOT deposited on a piece of SMF-28 fiber is connected to terminal 2 of the circulator by an AFC/PC connector. The back-reflected signal is measured through terminal 3 by a spectrometer or an Optical Spectrum Analyzer (OSA).

Optical Materials EXPRESS

It is important to realize that the back-reflection value is not the true reflection of PEDOT, and we need to consider absorption, attenuation, and transmission in the system to find the real value of reflection (refer to Eq. (1) Section 3.2). To measure transmission, the circulator is removed and the coated fiber is connected directly to the OSA by using a bare fiber connector. Knowing, the transmission and the reflection of PEDOT, the absorption coefficient for the nominated range of wavelengths can be determined.

Vis-NIR measurements are performed using an ANDO AQ-6315E OSA and NIR-SWIR measurements, with an Ocean Optic linear array spectrometer (NIRQUEST512-2-5). To measure reflection, an incoherent Laser Driven Light Source (LDLS EQ-99XFC) is used.

3. Results

3.1. Preparation of PEDOT:Tos coated fibers

In order to deposit small volumes of oxidant at the tip of an optical fiber, a liquid splitting method is developed. In this method, the oxidant solution is first dip coated at the end of an optical fiber (Fig. 3). This process leads to a volume of the oxidant solution at the tip of the fiber as well as the neighboring edges of the fiber. To reduce the volume, a second step was introduced to partially transfer the oxidant solution from the tip of the first optical fiber to another new optical fiber, by bringing them into contact and then retracting them (Fig. 3b to d). This step splits the oxidant between the tips of the two fibers. The splitting ratio between the two fibers relates to the difference in relative surface energy of the fibers themselves. The hypothesis here is that equal surface energy for each fiber leads to equal volumes of oxidant being split between them using the aforementioned process. This was confirmed in the case of two pristine fibers, and two plasma treated fibers. Conversely, different relative surface energy between the fibers yields uneven splitting. This was confirmed using one plasma treated fiber, and one pristine fiber. By controlling the surface energy of the fibers, as well as introducing subsequent splitting steps using more fibers, reasonable control over the volume of oxidant on the fiber for use can be achieved. After the splitting process, the oxidant initially exhibited a cone-shaped geometry. However, after a few minutes, the conical geometry collapsed and the oxidant formed the shape of a truncated sphere(refer to Fig. 3).

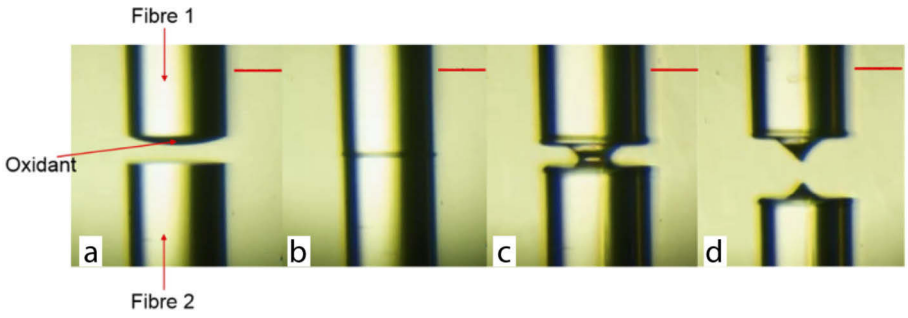

Fig. 3. Splitting method, (a) Optical fiber 1 dipped in oxidant solution, (b) transferring the oxidant onto optical fiber 2, (c) splitting the oxidant between two optical fibers, (d) oxidant successfully transferred onto the end of the optical fiber 2. Scale bars represent 50 μm (red line).

The oxidant coated fiber is then placed inside the VPP chamber for polymerization. After 30 minutes of polymerization time, the fiber is removed from the chamber for further post-processing. This is done by dropping a small number of droplets of EtOH on the VPP PEDOT:Tos coated fiber while the fiber is orientated vertically (PEDOT on top). This washing must be done carefully so as to remove all used oxidant and unreacted monomer material while not displacing the

Optical Materials EXPRESS

small PEDOT:Tos layer from the end of the fiber. Figure 4 shows the microscope images of the PEDOT:Tos formed after the polymerization process. SEM imaging illustrates the morphology of the PEDOT:Tos layer at the tip of the fiber (Fig. 4(c)). Any misalignment between fiber 1 and fiber 2 during the splitting process will result in non-concentric position of the oxidant solution on the fibers. In this scenario the truncated sphere shape of the oxidant layer is then replicated in the PEDOT:Tos formed after the VPP process, as evident from the interference fringes caused by multiple reflections at the air-film and film-optical fiber (Fig. 4(a) and (b)). By the introduction of micromachined fixtures to hold and position the fibers for alignment this problem was eliminated (Fig. 4(d)). This can be seen in the microscopic image in Fig. 4(b). Using the FIB/SEM, mechanical and optical profilometry measurements the thickness of PEDOT:Tos coating located on the core of the optical fiber was found to be between 200 to 500 nm.

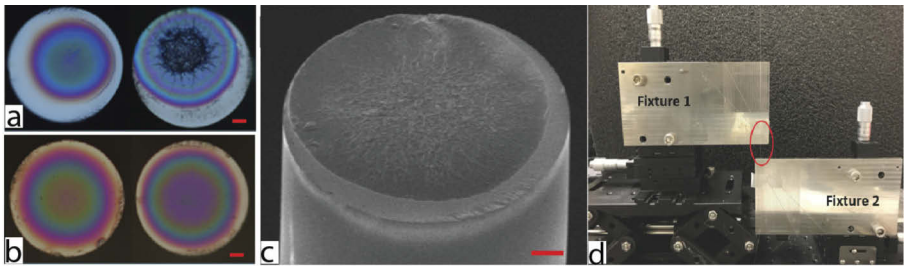

Fig. 4. Optical microscopic images (reflection mode) of PEDOT:Tos synthesised on various optical fibers (a) before, (b) after the introduction of smart fixtures for 3 dimensional alignment of fibers, (c) SEM image of PEDOT:Tos coated at the tip of an optical fiber, and (d) Micromachined fixtures designed for this project, the red oval display the location of fiber under test. Scale bars represent 15 μm (red line a-c).

Elemental molecular mapping using ToF-SIMS of an optical fiber coated with VPP PEDOT is shown in Fig. 5. The ToF-SIMS maps show the total negative (Fig. 5(a)) and positive (Fig. 5(e)) molecular and elemental fragments ejected from the polymer sample surface. Figure 5(b) is the signal from S- which could be fragments from either PEDOT or Tos molecules. Figure 5c which corresponds to the 171 amu peak, is the signal from $C_7H_7O_3S$- which is Tos by itself. The 187 amu peak (Fig. 5(d)) corresponds to the signal from $C_6H_6O_4S$-, which is attributed to a fragment of PEDOT (given the fragment mass is larger than Tos). The presence of Fe^{2+} at the perimeter of the PEDOT:Tos layer is observed (Fig. 5(f)). The residual Fe^{2+} comes from the original oxidant material that has not been completely washed from the sample and only resides at the edges of the PEDOT:Tos. Given the location of the Fe^{2+} away from the core, its presence is not expected to impact the subsequent optical analysis.

3.2. Optical measurements

Vis-NIR-SWIR from 400 to 2500 nm spectroscopy was used to determine the absorbance spectrum of a macroscopic area VPP PEDOT:Tos film prepared using spin-coated oxidant on a glass microscope slide (polymer thickness of 170±20 nm). To remove the glass substrate optical properties, the PEDOT:Tos thin film was removed from the glass and placed on top of an Al mesh (1 cm diameter holes) so the light focuses and passes through a hole where only the PEDOT:Tos layer is present. The result of the macroscopic thin film are compared in Fig. 6 with two samples of VPP PEDOT:Tos (200 to 250 nm thickness) coated at the tip of the optical fiber. For the fiber samples, absorbance data were collected from two different instruments covering a spectral range from 400 nm to 2300 nm. Both spectra follow the same trend with the transition of polaron and bipolaron states of charged carriers to a higher order of electron paired and unpaired states that results in a local minima at around 1100 nm as stated by Zozoulenko et. al [30]. The result of

Optical Materials EXPRESS

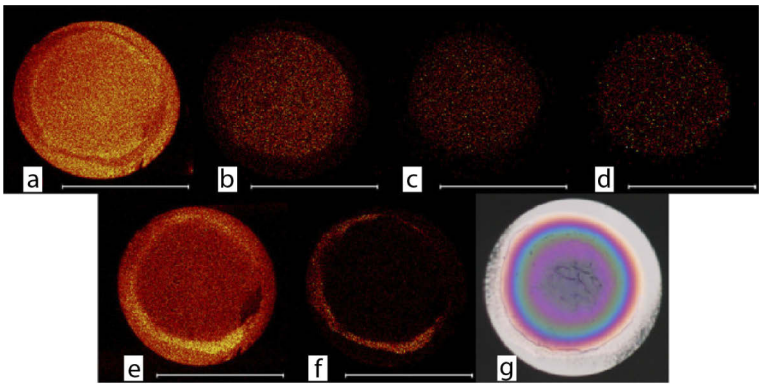

Fig. 5. ToF-SIMS results for VPP PEDOT:Tos coated fiber tip after fabrication: (a) -SIMS total ion, (b) S-, (c) Tosylate ($C_7H_7O_3S$-), (d) fragments of the PEDOT ($C_6H_6O_4S$-), (e) +SIMS total ion, (f) Fe^{2+}, (g) microscope image. Scale bars represent 100 μm (white line a-f).

thin film spectroscopy demonstrates an absorption increase in the SWIR region (1.4 - 2.4 μm) which is in line with the literature [31].

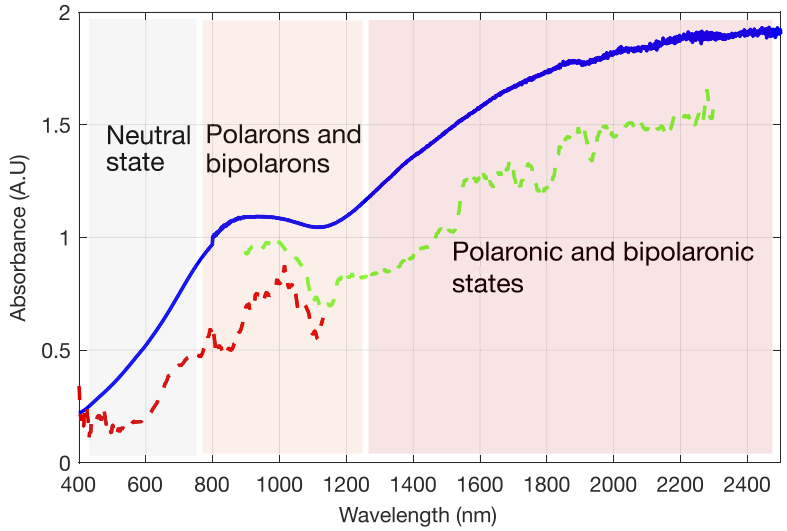

Fig. 6. Comparison of absorbance of thin layer (170 nm - blue line) of macroscopic area (~ 4 cm^2) VPP PEDOT:Tos and microscale (~ 100 μm^2) VPP PEDOT:Tos at the tip of the optical fiber. Red dashed line measured with ANDO Optical Spectrum Analyzer, and green dashed line measured with Ocean Optic linear array spectrometer. For reference, the electrical conductivity of the macroscopic area thin film was measured to be ca. 1800 S/cm.

Ellipsometry is a well-established technique used to determine the optical constants of anisotropic material such as PEDOT:PSS [32]. However, the smallest beam diameters are typically about 2 mm^2, noting though advanced optics can achieve spot sizes of ca. 100 μm, and also the optical modeling to analyze the measured data is complex due to the high sensitivity of phase shift difference. Herein, we present a method to find the reflection of the microscale volume VPP PEDOT:Tos. A Laser-Driven Light Source (LDLS) is coupled to a circulator and both the back-reflection by the PEDOT:Tos and transmission through polymer were measured

Optical Materials EXPRESS

around 1550 nm of λ. A setup similar to the one in Fig. 2(b) was used to measure the reflection spectra and absorption coefficient of a 200 nm thickness PEDOT:Tos layer deposited at the tip of a SMF-28 fiber. A LDLS (incoherent light source) was introduced to eliminate intensity variations due to the coherence of the SC source. By conducting a series of measurements using a fiber coupled LDLS, the transmission and back-reflection spectra of the circulator were measured for all combinations of 1↦2, 2↦3 and 1↦3 and vice versa (first number being input and second number output of the circulator). These spectra then have been used to calculate the response function of the circulator, i.e., C_{12}, C_{23} and C_{13} using which the reflection spectra of the PEDOT layer (Fig. 7) can be found as:

$$P_3(\lambda) = P_1(\lambda)C_{12}R_{\mathrm{PEDOT}}C_{23} + P_1(\lambda)C_{13}, \tag{1}$$

where $P_3(\lambda)$ is the output power of the circulator, $P_1(\lambda)$ is the input power, C_{12}, C_{23} and C_{13} are circulator response from 1 to 2, 2 to 3 and 1 to 3 respectively (Fig. 7.a) and R_{PEDOT} is the reflectivity of VPP PEDOT:Tos (Fig. 7(b)). To prevent damaging the PEDOT:Tos at the tip of the fiber, when exposed to a broadband laser spectrum, a low input power (< 1 mW) is applied. For such input power, the amount of light transmitted through the tip and measured by the spectrometer is below the measurement limit of the device. Therefore, we consider the transmitted power to be negligible with respect to those of the reflected and absorbed ones. The reflection spectrum in here is mainly due to the first interface of the sample, i.e the fiber/PEDOT:Tos interface, as the material has high absorbance at NIR. The error in back-reflection is mainly due to light interference at that interference and is measured to be less than 3%. The reflection was measured between 1200 nm to 1700 nm of wavelength with resolution of 1 nm. The results represent the increase in reflection and decrease in absorption at longer wavelengths.

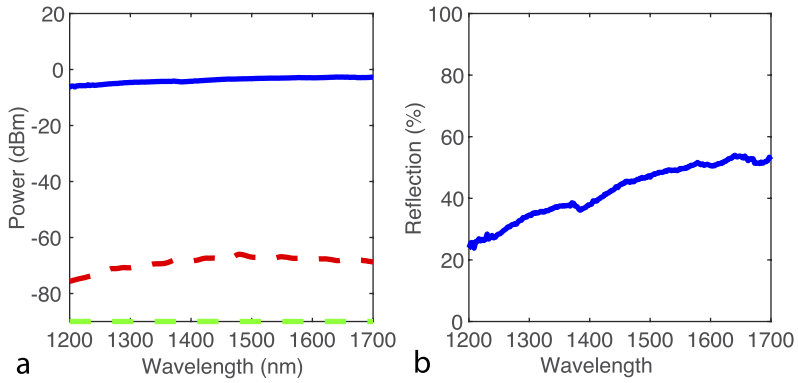

Fig. 7. (a) Optical circulator response: Blue line is the input broadband light intensity to the terminal 1. Red dashed line represents circulator response C_{12} and C_{23}. Green dashed line is the circulator response C_{13} and C_{31} , (b) PEDOT:Tos reflection spectrum.

By varying the laser power irradiated onto the layer the VPP PEDOT:Tos layer we can control the degradation time (the time prior to transmission increases significantly) at the single wavelength of λ=1550 nm over an exposure time of 8 hr. Significantly here is defined as 5% of maximum transmission if the maximum reach the 10% of input power. Figure 8(a), illustrates the transmission response of the VPP PEDOT:Tos with increasing CW laser power as a function of time. At light intensities below 5 mW, a small change (<2%) in the transmitted power over an 8 hr period is noticed, indicating that almost all of the laser power is absorbed and reflected by the PEDOT:Tos. As the incident laser power is increased above 5 mW, an increase in the transmission is observed, albeit after a time period of no change. The time taken to reach the onset of transmission increase, decreases as the power of the CW laser is increased (Fig. 8(c)).

Optical Materials EXPRESS

Hereafter, the level at which the material starts to degrade and permanently change its optical properties will be called the laser-induced damage threshold (LIDT). laser-induced damage (LID) scatters light thus damaging the structure of the material in the vicinity of the core, and after some time the damage spreads through the material [33–35].

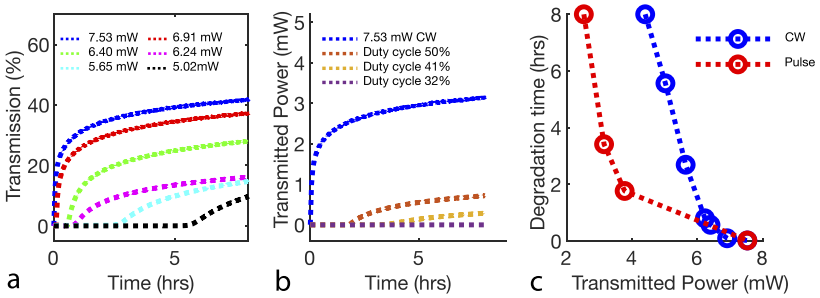

Fig. 8. (a) Measured transmitted power through the PEDOT:Tos (transmission) coated fiber at different CW powers normalized to the input power as a function of time, (b) Measured average transmitted power as the function of time for CW and pulsed laser with constant peak power. The plot shows the effect of different pulse duration at 1550 nm on degradation time. The degradation time increase as the off time period increases. This is demonstrated for pulse widths of 6.8μs (50% duty cycle), 5.58μs (41% duty cycle) and 4.35μs (32% duty cycle) with 7.53 mW peak power and 13.6 μs period (pulse repetition rate of 73.529 kHz) as fixed parameters. (c) Comparison of degradation time with average transmitted power for CW and pulsed laser obtained from part a and b.

In order to understand the mechanism by which the transmission of the VPP PEDOT:Tos increases, ToF-SIMS mapping was conducted on a sample after being exposed to a laser power > 5 mW for 8 hr. Figure 9 shows the total negative and positive fragments on the sample surface respectively. Figure 9(b) and 9(c) shows the signal from S and Tos. Significant decrease in ion concentration can be observed for both S and Tos when compared to the corresponding concentration in the unirradiated sample (Fig. 5). Moreover, there is practically no signal related to that of PEDOT:Tos. This shows that the polymer has been decomposed into the constituent atoms that make up PEDOT:Tos. More importantly, the mapping shows the chemistry what is left behind is quite uniform across the surface of the optical fiber. This finding is in contrast with the optical microscopic image, highlighting a physically different region aligned with the core of the fiber (bright spot in Fig. 9(f)). Furthermore, the optical microscopic image shows optical interference bands indicative of a thin film still being present. The very nature of this contrasting chemical versus physical degradation will be the focus of subsequent studies. Herein, it is proposed that the VPP PEDOT:Tos undergoes some form of opto-thermal degradation as the optically deposited energy increases due to incident laser light.

Stability, recovery, and lifetime are important parameters for practical applications of VPP PEDOT:Tos coated fibers. Thermal degradation of bulk PEDOT:PSS has been studied by different groups [36–38] and the results show that PEDOT:PSS is stable up to approximately 110 °C [39]. In the case of PEDOT:Tos, Winter-Jensen and co-workers [38] demonstrated that heating beyond 150 °C under atmospheric conditions induces structural change within PEDOT:Tos that can be observed as changes in the electrical conductivity. However, to the best of our knowledge, this is the first report that investigates the time degradation of PEDOT:Tos at sub-micro scale at the tip of the fiber due to the exposure of laser irradiation.

To further investigate the parameters that affect this opto-thermal effect, we have undertaken a series of experiments with a pulsed laser with a constant period of 13.6 μs (Fig. 8(b)). The pulse lengths widths longer than 1 μs can be treated as CW lasers for LIDT purposes [40].

Optical Materials EXPRESS

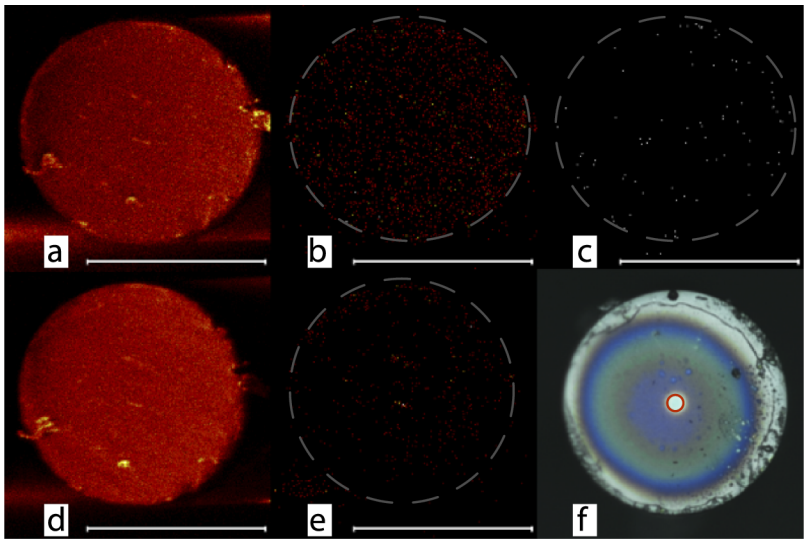

Fig. 9. ToF-SIMS results after exposure to 1550 nm for 8 hr (a) -SIMS Total ion, (b) S-, (c) Tosylate ($C_{-}7H_{-}7O_{-}3S$-), (d) +SIMS Total ion, (e) Fe^{2+}, (f) microscopic image shows LID features in the core of 8.2 μm (red circle) and surrounding area on an ~300 nm thickness PEDOT:Tos sample at the core of the fiber irradiated at 88.6±0.2 W/mm^2 over irradiation time of 8 hr. Scale bars represent 100 μm (white line a-e).

In this experiment, the peak power of the laser was held constant and the duty cycle of the pulsed laser varied. The first observation from Fig. 8(b) is that using a pulsed laser instead of a CW laser increases the degradation time in PEDOT:Tos. Decreasing the duty cycle (less time 'on', more time 'off') further delays the degradation time. In the case of a 32% duty cycle, there are no change in the optical properties observed across an 8 hr experiment. In a semi-quantitative analysis, this implies that the rate at which the PEDOT:Tos dissipates energy (radiative and conduction loss of energy) is halved compared to the rate of energy accumulation in the PEDOT:Tos. This interpretation of accumulation and dissipation of energy will be tested in the following section. We hypothesize that this opto-thermal effect is based on the energy of laser light incident on the layer is deposited into the layer via absorption while the dissipation of energy due to thermal conduction and heat radiation, reduces the energy of the layer. We think that interplay between absorbed energy and dissipated energy is the leading factor in the determination of the degradation time. To further investigate this hypothesis, in the next section we develop a mathematical model.

3.3. Mathematical model

Here, we develop a new mathematical model based on energy deposition in the PEDOT:Tos layer. We hypothesize that the rate of change of energy due to the exposure to a laser beam, at any certain time, depends on the optical absorption of the PEDOT:Tos layer (Eq. (2)). Hence, we write:

$$\frac{dE}{dt} = \frac{\alpha P}{k} - \frac{\beta E}{k}, \tag{2}$$

where α is the absorption of the layer of the VPP PEDOT:Tos, P (mW) is the laser power, β (1/s) is the rate of decay, E (mJ) is the energy of the layer, and k is the proportionality constant between absorption and the rate of decay. By knowing that the sum of the transmission, reflection, and absorption in the absence of nonlinear effects is equal to unity [41], herein, the fraction of light absorbed by the layer α obtained to be 0.504 for a wavelength of 1550 nm from the previous

Optical Materials EXPRESS

figure (Fig. 7b). Taking the integral of both sides of Eq. 2, assuming constant P and initial layer energy of E_0, one can find the general solution to the equation as:

$$E = \frac{\alpha}{\beta}P(1 - exp[\frac{-\beta t}{k}]) + E_0 exp[\frac{-\beta t}{k}]. \tag{3}$$

Defining the threshold energy, E_{th}, as energy at which the layer starts to degrade, we can find the time that takes to reach degradation, t_{deg}, for a CW laser beam. By assuming $E_0 = 0$, we have:

$$t_{deg} = -B(\ln[1 - \frac{A}{\alpha P}]), \tag{4}$$

where $A = \beta E_{th}$ (mJ/s) and $B = k/\beta$ (s). These constant coefficients, A and B are considered as free parameters of the model that need to be determined by fitting to experimental results. Using the degradation times corresponding to different CW laser powers in Fig. 8a to fit to Eq. (4), we can find values of A and B from experimental results as shown in Fig. 10. The value of A depends on the lowest power at which VPP PEDOT:Tos degrades. The lowest power in the graph represents a PEDOT:Tos exposed to 4.8 mW CW laser for approximately 19 hr before degradation happens, noting that this is highly dependent on the thickness of the sample. The fit in Fig. 10, is associated with R-squared of 96% based on which the values of A and B are 2.41 mJ/s (fixed at the upper boundary of natural log) and 1.236 hr respectively. Due to the properties of natural log the fitting algorithm will always match the last data point as natural log function can not go below zero. Hence, there is an uncertainty in the fitting procedure. We can achieve R-squared fitting of above 95% within the range of A (2.1 to 2.4 mJ/s) and B (1.24 - 1.69 hr).

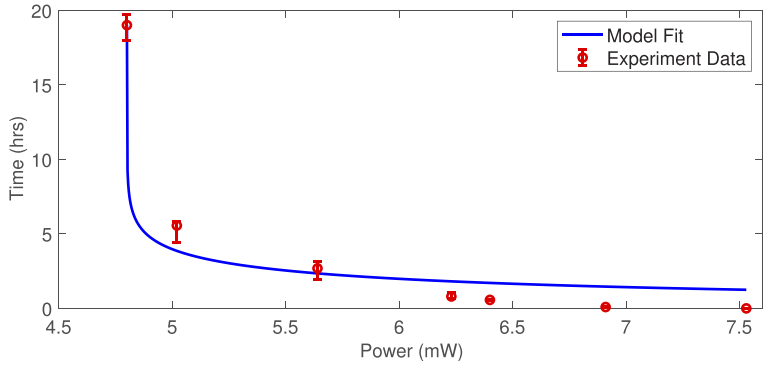

Fig. 10. Degradation time as a function of laser CW power. Red dots with error bars represent the experimental data and the blue line represents the model fit to CW experimental data using Eq. 4.

The mathematical model can be extended to include a train of square pulses by successively applying Eq. 3 for accumulative initial energies E_0 (as shown in the inset in Fig. 11, red square pulses). In this case, the VPP PEDOT:Tos layer experiences both absorption and decay of energy during the on-time period, while only experiencing energy decay during off-time periods. It can be shown that after N successive periods we find:

$$A_N = \alpha P(1 - exp(\frac{-t_0}{B}))exp(\frac{-\Delta t}{B})[\frac{1 - exp(\frac{-NT}{B})}{1 - exp(\frac{-T}{B})}], \tag{5}$$

where $A_N = \beta E_N$, E_N is the energy of the layer after N successive pulse, t_0 is the pulse on-time, Δt is the off-time of the signal and $T = t_0 + \Delta t$ is the period of the signal. B is the constant

Optical Materials EXPRESS

fitting parameter obtained by fitting to CW results for the associated PEDOT:Tos layer. Hence, once determined through fitting to CW results, it can be used in Eq. (5), within the uncertainty of the experiment and model approximation. Figure 11 shows the time evolution of A_N as a function of time for laser pulses with different duty cycles of 50%, 41% and 32% (similar to Fig. 8(b)). Using the experimental degradation times for 50% (t_{deg1}) and 41% (t_{deg2}) duty cycles from Fig. 8(b), we can find the threshold values of A_N, as shown by horizontal dotted lines in Fig. 11. Note that using the experimental degradation times for 50% and 41% duty cycles (from Fig. 8(b)), results in a consistent threshold values of A_N within 1.42±0.06 mJ/s or range of 4%. This indicates the validity of our model within the restriction of the approximation used for the model. In addition, the curve for 32% duty cycle indicates that the sample should not degrade as the equilibrium A_N value is below the threshold value, which is consistent with the experimental observation showing no degradation for 32% duty cycle pulses (purple dotted line Fig. 8(b)). Considering Eq. (4), we find that for $\alpha P < A_N$ threshold, the degradation time is undefined. This suggest that for A_N threshold divided by absorption coefficient (α) is the average threshold power (P_{th}) below which no degradation occurs. Identifying threshold power is practically important since by choosing right laser pulse parameters, such that $P_{ave} < P_{th}$, one can avoid LID in the PEDOT:Tos layer. In here, we find $P_{th} = 2.82 \pm 0.12$.

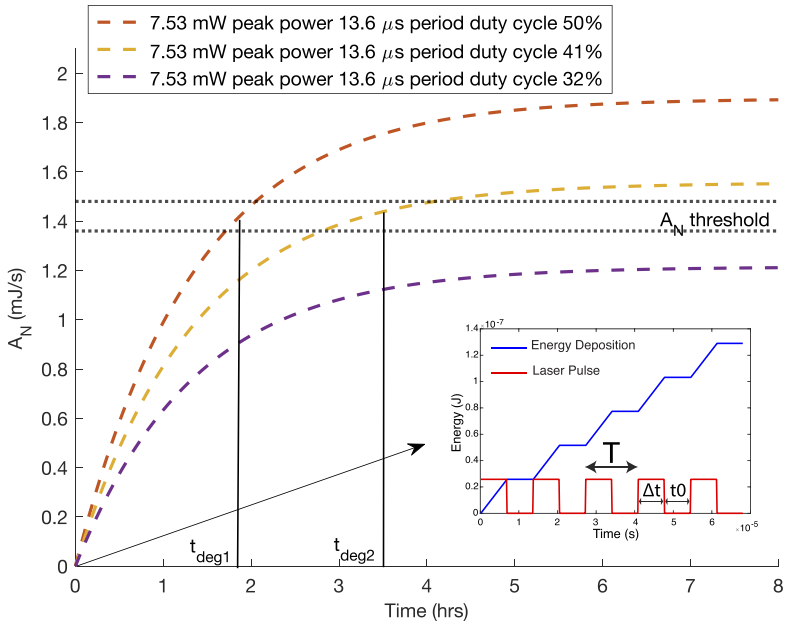

Fig. 11. Energy deposited into the layer as a function of pulsed laser irradiation based on the mathematical model for pulse peak power 7.53 mW, the model reach the 1.44 mJ/s LIDT for B = 1.33. A_N threshold for laser pulse simulation obtained by putting lower and upper value of B threshold (1.24 - 1.69 hr). t_{deg1} = 1.868 (hr) and t_{deg2} = 3.491 (hr) obtained from brown and yellow dotted line in Fig. 8(b) respectively. The inset figure demonstrate the simulation of the first 5 pulses of the simulation. The blue line illustrates energy deposition and energy dissipation by letting β = 500 (1/s) into Eq. (3).

It is also noted that the range of values of A_N threshold obtained from pulsed model (1.36 to 1.48 mJ/s) is different from the one obtained from CW model (2.1 to 2.4 mJ/s). This discrepancy can be due to the thickness variation between samples (in degradation experiments herein this was 350 - 500 nm) and the assumptions in the model that the absorption is constant before degradation. It is possible that the absorption itself is a function of energy before the degradation

Optical Materials EXPRESS

time. While this function can be initially approximated by a linear function, it can be nonlinear close to the LIDT, hence, lowering the LIDT of PEDOT:Tos. Such a nonlinear absorption has been reported mainly in semiconducting materials [42]. Another potential contributing factor could be due to the fact that for pulses shorter than <0.1 ms LID breakdown can occur due to both the dielectric and thermal breakdowns [43]. Overall, absorption of the optical radiation is the main cause of LID for long pulse and CW laser [42]. In general, different mechanisms can contribute to optical absorption such as transient, localized (impurities), surface and subsurface (surface Roughness, waviness, imperfections) absorption which can explain the difference of CW and pulsed laser data.

4. Conclusion

In this study, we successfully prepared and fabricated VPP PEDOT:Tos on the tip of single mode optical fibers. These coated fibers are then subject to optical transmission and reflection measurements to determine the absorbance, reflectance and laser-induced damage (LID) threshold of VPP PEDOT:Tos. Understanding the optical behavior of micro-scale volumes of VPP PEDOT:Tos is essential for developing fiber optic sensing systems that use conducting polymers as the sensing material. For both CW and laser pulses, the LID was observed in the PEDOT:Tos where the degradation time defined as the time when the transmission suddenly increases. A mathematical model was developed to understand the degradation in the CW regime based on the experimental results. The mathematical model was also applied to the pulsed laser results for the degradation based on energy accumulated and dissipated in the layer. According to the mathematical model we were able to estimate the average power below which LID can be avoided. This is important for practical applications since it allows the laser parameters to be chosen in order to avoid degradation of the PEDOT:Tos layer. To avoid LID at a wavelength of 1550 nm, in low peak power regime ($\leqslant$ 7.53 mW), we suggest that irradiance should not exceed 31.8 W/mm^2 (average power lower limit 2.70 mW with a mode field diameter of 10.4±0.5 μm).

Funding

Australian Research Council (DP170104367, FT160100300); Commonwealth Government of Australia Research Training Program (RTP).

Acknowledgments

This work was performed in part at the South Australian and the Optofab node of the Australian National Fabrication Facility under the National Collaborative Research Infrastructure Strategy. S. SHAHNIA acknowledges the support of Australian Government through a scholarship under the Australian Research Council discovery project (DP170104367). J. Rehmen acknowledges the support of the Australian Government through a scholarship under the Research Training Program. T. M. Monro acknowledges the support of an ARC Georgina Sweet Laureate Fellowship. D. Evans acknowledges the support of the Australian Research Council through FT160100300.

References

1. M. Mueller, M. Fabretto, D. Evans, P. Hojati-Talemi, C. Gruber, and P. Murphy, "Vacuum vapour phase polymerization of high conductivity pedot: Role of PEG-PPG-PEG, the origin of water, and choice of oxidant," Polymer **53**(11), 2146–2151 (2012).
2. K. Zuber, M. Fabretto, C. Hall, and P. Murphy, "Improved pedot conductivity via suppression of crystallite formation in fe (iii) tosylate during vapor phase polymerization," Macromol. Rapid Commun. **29**(18), 1503–1508 (2008).
3. E. Nasybulin, W. Xu, M. H. Engelhard, X. S. Li, M. Gu, D. Hu, and J.-G. Zhang, "Electrocatalytic properties of poly(3,4-ethylenedioxythiophene) (pedot) in Li-O_2 battery," Electrochem. Commun. **29**, 63–66 (2013).
4. P. P. Cottis, D. Evans, M. Fabretto, S. Pering, P. Murphy, and P. Hojati-Talemi, "Metal-free oxygen reduction electrodes based on thin pedot films with high electrocatalytic activity," RSC Adv. **4**(19), 9819–9824 (2014).

Optical Materials EXPRESS

5. I. D. Norris, M. M. Shaker, F. K. Ko, and A. G. MacDiarmid, "Electrostatic fabrication of ultrafine conducting fibers: polyaniline/polyethylene oxide blends," Synth. Met. **114**(2), 109–114 (2000).
6. C. Pozo-Gonzalo, D. Mecerreyes, J. A. Pomposo, M. Salsamendi, R. Marcilla, H. Grande, R. Vergaz, D. Barrios, and J. M. Sánchez-Pena, "All-plastic electrochromic devices based on pedot as switchable optical attenuator in the near ir," Sol. Energy Mater. Sol. Cells **92**(2), 101–106 (2008).
7. E. Poverenov, M. Li, A. Bitler, and M. Bendikov, "Major effect of electropolymerization solvent on morphology and electrochromic properties of pedot films," Chem. Mater. **22**(13), 4019–4025 (2010).
8. A. Kumar, D. M. Welsh, M. C. Morvant, F. Piroux, K. A. Abboud, and J. R. Reynolds, "Conducting poly(3,4-alkylenedioxythiophene) derivatives as fast electrochromics with high-contrast ratios," Chem. Mater. **10**(3), 896–902 (1998).
9. O. Bubnova, Z. U. Khan, H. Wang, S. Braun, D. R. Evans, M. Fabretto, P. Hojati-Talemi, D. Dagnelund, J.-B. Arlin, Y. H. Geerts, S. Desbief, D. W. Breiby, J. W. Andreasen, R. Lazzaroni, W. M. Chen, I. Zozoulenko, M. Fahlman, P. J. Murphy, M. Berggren, and X. Crispin, "Semi-metallic polymers," Nat. Mater. **13**(2), 190–194 (2014).
10. C. Yi, L. Zhang, R. Hu, S. S. C. Chuang, J. Zheng, and X. Gong, "Highly electrically conductive polyethylenedioxythiophene thin films for thermoelectric applications," J. Mater. Chem. A **4**(33), 12730–12738 (2016).
11. M. Kateb, V. Ahmadi, and M. Mohseni, "Fast switching and high contrast electrochromic device based on pedot nanotube grown on zno nanowires," Sol. Energy Mater. Sol. Cells **112**, 57–64 (2013).
12. J. Kawahara, P. A. Ersman, I. Engquist, and M. Berggren, "Improving the color switch contrast in PEDOT:PSS-based electrochromic displays," Org. Electron. **13**(3), 469–474 (2012).
13. V. S. Vasantha and S.-M. Chen, "Electrochemical preparation and electrocatalytic properties of pedot/ferricyanide film-modified electrodes," Electrochim. Acta **51**(2), 347–355 (2005).
14. T. Nguyen, P. Le Rendu, P. Long, and S. De Vos, "Chemical and thermal treatment of PEDOT:PSS thin films for use in organic light emitting diodes," Surf. Coat. Technol. **180-181**, 646–649 (2004).
15. Z. Hu, J. Zhang, and Y. Zhu, "Effects of solvent-treated PEDOT:PSS on organic photovoltaic devices," Renewable Energy **62**, 100–105 (2014).
16. D. Bernards, D. Macaya, M. Nikolou, J. Defranco, S. Takamatsu, and G. Malliaras, "Enzymatic sensing with organic electrochemical transistors," J. Mater. Chem. **18**(1), 116–120 (2008).
17. R. Brooke, P. Cottis, P. Talemi, M. Fabretto, P. Murphy, and D. Evans, "Recent advances in the synthesis of conducting polymers from the vapour phase," Prog. Mater. Sci. **86**, 127–146 (2017).
18. R. Brooke, E. Mitraka, S. Sardar, M. Sandberg, A. Sawatdee, M. Berggren, X. Crispin, and M. P. Jonsson, "Infrared electrochromic conducting polymer devices," J. Mater. Chem. C **5**(23), 5824–5830 (2017).
19. A. Weathers, Z. U. Khan, R. Brooke, D. Evans, M. T. Pettes, J. W. Andreasen, X. Crispin, and L. Shi, "Significant electronic thermal transport in the conducting polymer poly (3, 4-ethylenedioxythiophene)," Adv. Mater. **27**(12), 2101–2106 (2015).
20. B. Cho, K. S. Park, J. Baek, H. S. Oh, Y.-E. Koo Lee, and M. M. Sung, "Single-crystal poly (3, 4-ethylenedioxythiophene) nanowires with ultrahigh conductivity," Nano Lett. **14**(6), 3321–3327 (2014).
21. R. Brooke, M. Fabretto, N. Vucaj, K. Zuber, E. Switalska, L. Reeks, P. Murphy, and D. Evans, "Effect of oxidant on the performance of conductive polymer films prepared by vacuum vapor phase polymerization for smart window applications," Smart Mater. Struct. **24**(3), 035016 (2015).
22. J. R. Reynolds, A. Kumar, J. L. Reddinger, B. Sankaran, S. A. Sapp, and G. A. Sotzing, "Unique variable-gap polyheterocycles for high-contrast dual polymer electrochromic devices," Synth. Met. **85**(1-3), 1295–1298 (1997).
23. J. O. Norris, "Current status and prospects for the use of optical fibres in chemical analysis. a review," Analyst **114**(11), 1359 (1989).
24. S. Musolino, E. P. Schartner, G. Tsiminis, A. Salem, T. M. Monro, and M. R. Hutchinson, "Portable optical fiber probe for in vivo brain temperature measurements," Biomed. Opt. Express **7**(8), 3069–3077 (2016).
25. M. Tabib-Azar, B. Sutapun, R. Petrick, and A. Kazemi, "Highly sensitive hydrogen sensors using palladium coated fiber optics with exposed cores and evanescent field interactions," Sens. Actuators, B **56**(1-2), 158–163 (1999).
26. R. Kostecki, H. Ebendorff-Heidepriem, S. Afshar, G. McAdam, C. Davis, and T. M. Monro, "Novel polymer functionalization method for exposed-core optical fiber," Opt. Mater. Express **4**(8), 1515–1525 (2014).
27. R. Brooke, D. Evans, M. Dienel, P. Hojati-Talemi, P. Murphy, and M. Fabretto, "Inkjet printing and vapor phase polymerization: patterned conductive pedot for electronic applications," J. Mater. Chem. C **1**(20), 3353–3358 (2013).
28. C. D. O'Connell, M. J. Higgins, H. Nakashima, S. E. Moulton, and G. G. Wallace, "Vapor phase polymerization of edot from submicrometer scale oxidant patterned by dip-pen nanolithography," Langmuir **28**(26), 9953–9960 (2012).
29. J. Edberg, D. Iandolo, R. Brooke, X. Liu, C. Musumeci, J. W. Andreasen, D. T. Simon, D. Evans, I. Engquist, and M. Berggren, "Patterning and conductivity modulation of conductive polymers by UV light exposure," Adv. Funct. Mater. **26**(38), 6950–6960 (2016).
30. I. ozoulenko, A. Singh, S. K. Singh, V. Gueskine, X. Crispin, and M. Berggren, "Polarons, bipolarons, and absorption spectroscopy of PEDOT," ACS Appl. Polym. Mater. **1**(1), 83–94 (2019).
31. N. Massonnet, A. Carella, O. Jaudouin, P. Rannou, G. Laval, C. Celle, and J.-P. Simonato, "Improvement of the seebeck coefficient of PEDOT:PSS by chemical reduction combined with a novel method for its transfer using free-standing thin films," J. Mater. Chem. C **2**(7), 1278–1283 (2014).
32. L. A. Pettersson, F. Carlsson, O. Inganäs, and H. Arwin, "Spectroscopic ellipsometry studies of the optical properties of doped poly (3, 4-ethylenedioxythiophene): an anisotropic metal," Thin Solid Films **313-314**, 356–361 (1998).

Optical Materials EXPRESS

33. F. Y. Genin, M. D. Feit, M. R. Kozlowski, A. M. Rubenchik, A. Salleo, and J. Yoshiyama, "Rear-surface laser damage on 355-nm silica optics owing to fresnel diffraction on front-surface contamination particles," Appl. Opt. **39**(21), 3654–3663 (2000).
34. C. Carr, M. Matthews, J. Bude, and M. Spaeth, "The effect of laser pulse duration on laser-induced damage in kdp and Si-O_2," in *Laser-Induced Damage in Optical Materials: 2006*, vol. 6403 (International Society for Optics and Photonics, 2007), p. 64030K.
35. J.-Y. Natoli, L. Gallais, H. Akhouayri, and C. Amra, "Laser-induced damage of materials in bulk, thin-film, and liquid forms," Appl. Opt. **41**(16), 3156–3166 (2002).
36. L. Stepien, A. Roch, R. Tkachov, B. Leupolt, L. Han, N. van Ngo, and C. Leyens, "Thermal operating window for pedot:pss films and its related thermoelectric properties," Synth. Met. **225**, 49–54 (2017).
37. E. Vitoratos, S. Sakkopoulos, E. Dalas, N. Paliatsas, D. Karageorgopoulos, F. Petraki, S. Kennou, and S. Choulis, "Thermal degradation mechanisms of PEDOT:PSS," Org. Electron. **10**(1), 61–66 (2009).
38. I. Winter, C. Reese, J. Hormes, G. Heywang, and F. Jonas, "The thermal ageing of poly(3,4-ethylenedioxythiophene). an investigation by X-ray absorption and X-ray photoelectron spectroscopy," Chem. Phys. **194**(1), 207–213 (1995).
39. M. Hokazono, H. Anno, and N. Toshima, "Thermoelectric properties and thermal stability of PEDOT:PSS films on a polyimide substrate and application in flexible energy conversion devices," J. Electron. Mater. **43**(6), 2196–2201 (2014).
40. R. Wood, "Laser induced damage thresholds and laser safety levels. Do the units of measurement matter?" Opt. Laser Technol. **29**(8), 517–522 (1998).
41. J. M. Palmer, "The measurement of transmission, absorption, emission, and reflection," Handb. Optics **2**, 25 (1995).
42. R. M. Wood, *Laser-induced Damage of Optical Materials* (CRC Press, 2003).
43. R. M. Wood, *The Power-and Energy-handling Capability of Optical Materials, Components, and Systems*, vol. 60 (Spie Press, 2003).